

**Integrating Reduced Graphene Oxide with Microwave-Subcritical Water for Cellulose Depolymerization**

Journal:	<i>Catalysis Science &amp; Technology</i>
Manuscript ID	CY-ART-05-2018-000953.R1
Article Type:	Paper
Date Submitted by the Author:	19-Jul-2018
Complete List of Authors:	Mission, Elaine; Kumamoto Daigaku, Graduate School of Science and Technology Quitain, Armando ; Kumamoto University, Applied Chemistry and Biochemistry Yudai, Hirano; Kumamoto University, Graduate School of Science and Technology Sasaki, Mitsuru; Kumamoto University, Graduate School of Science and Technology Cocero, Maria Jose; Valladolid University, Chemical Engineering Kida, Tetsuya; Kumamoto University, Applied Chemistry and Biochemistry



Journal Name

ARTICLE

## Integrating Reduced Graphene Oxide with Microwave-Subcritical Water for Cellulose Depolymerization

Received 00th January 20xx,  
Accepted 00th January 20xx

DOI: 10.1039/x0xx00000x

www.rsc.org/

Elaine G. Mission<sup>a</sup>, Armando T. Quitain<sup>b,c\*</sup>, Yudai Hirano<sup>a</sup>, Mitsuru Sasaki<sup>d</sup>, Maria Jose Cocero<sup>e</sup>, and Tetsuya Kida<sup>b\*</sup>

Catalyst design and surface chemistry have been long regarded as the major foundation for the catalytic activity of carbon-based catalysts. However, surface modification of carbon-based catalysts typically involve huge quantities of strong acids that eventually leach in the solution contaminating target compounds. We have previously demonstrated that the mixture of reduced graphene oxide (rGO) and residual cellulose would generate additional glucose after the first cycle by simply elevating temperature. In this study we sought to understand how rGO under microwave (MW)-subcritical water (subH<sub>2</sub>O) facilitates the depolymerization of cellulose. It was found out that the MW sensitizing properties of rGO improved, enhancing the electronic transport properties. The partial removal of functional groups has resulted into much smaller particles and formation of nanopores and nanovoids which facilitated the precise cleaving of the glycosidic bonds with glucose yield reaching up to 66 ± 4 wt% in as short as 5 min. The yield highly correlates with the H<sub>3</sub>O<sup>+</sup>/OH<sup>-</sup> concentration and hugely depends on the rGO structure that varies according to the synthesis method, preferably in the absence of water. The depolymerization mechanism takes place via random scission. This study indicates that rGO, in spite of having fewer functionalities than pristine graphene oxide (GO), can still be used for catalysis even without surface modification in combination with MW and subH<sub>2</sub>O.

### 1. Introduction

Solid acid catalysts has been extensively studied to enable efficient pathways for biomass conversion into biofuels and oxychemicals<sup>1,2</sup>. One of the most intensively studied method is the hydrolysis of cellulose into fermentable sugars such as glucose, typically achieved through strong homogeneous acids and more recently, through heterogeneous acid catalysis. Particular interest has been devoted to carbon-based heterogeneous catalysts as metal-free and sustainable catalytic materials for cellulose depolymerization<sup>3</sup>. Cheaper biomass feedstock categorized as second-generation biomass would enable a cost competitive process, with additional cost cut from cheaper carbon-based catalysts than their metal-based counterparts<sup>4</sup>. The catalytic activity of carbon-based catalysts is governed by their design and surface chemistry, especially

by the presence of Bronsted-acid sites that play a huge role for the hydrolysis reaction. Rinaldi and Schuth has also discussed the importance of catalyst composition, active sites, water resistance and porosity for the design of solid catalysts<sup>5</sup>. Since acid density highly correlates to the catalytic activity<sup>7,8</sup>, various techniques on surface modification has been carried out in order to increase the density of acid sites onto the carbon backbone. Typical examples include sulfonation with sulfuric acids<sup>9</sup> and functionalization with halides or carboxylic acids<sup>10,11</sup>. Unfortunately, surface modification requires significant quantity of acids for preparation, and yet, catalyst reusability is limited. For instance, since the sulfo group leaches out, contaminating the target products<sup>12</sup>. It should also be noted that reactions involving water catalysed by solid acid, is a grand challenge for heterogeneous catalysis since it induce significant structural changes in the catalyst. Hence at some point, a trade-off between stability and activity must be enforced.

Amongst carbon-based catalysts, graphene oxide (GO) has attracted significant attention due to the variety of oxygenated functionalities in its surface while bearing the myriad of physical, chemical and electrical properties of graphene. We have previously demonstrated that the oxygenated functionalities on the GO surface, despite being weakly acidic, can synergistically disrupt the extensive hydrogen bonding network protecting the β-glycosidic bond for hydrolytic cleaving<sup>6</sup>. However, GO sheds off some surface functionalities under hydrothermal conditions, resembling reduced graphene oxide (rGO), which resulted to a slow-down on decrystallization of cellulose surface and cannot fully hydrolyze cellulose with the same activity as fresh GO.

<sup>a</sup> Graduate School of Science and Technology

<sup>b</sup> Faculty of Advanced Science and Technology

<sup>c</sup> College of Cross-Cultural and Multidisciplinary Studies

<sup>d</sup> Institute of Pulsed Power Science

Kumamoto University, Kumamoto 860-8555, Japan

<sup>e</sup> Department of Chemical Engineering and Environmental Technology, University of Valladolid, Valladolid 47001, Spain

† Electronic Supplementary Information (ESI) available: C1s and O1s XPS spectra of graphene oxide (GO), rGO1 (microwave-hydrothermal reduced GO) and rGO2 (thermally annealed GO); Combustion Elemental Analysis for GO, rGO1 and rGO2; Representative high performance liquid chromatography (HPLC) spectra for the combinations used in this study; Product distribution table in wt% yields; Glucose production from cellulose by various carbon materials; Spent rGO2 characterization (FTIR, XRD and XPS); and Particle size analysis of oligosaccharides

A major interest arising then is how carbon based catalysts without further functionalization with strong acids, could facilitate cellulose depolymerization. In the case of rGO, the reduced quantity of surface functionalities boosted its hydrophobicity, limiting its interaction with water and soluble compounds thus affecting efficiency of the depolymerization process. Instead of increasing the reactivity of cellulose that would require additional solvent or additive, we propose that the reactivity of water be amplified by increasing operating temperatures i.e. at subcritical conditions under MW irradiation. The large ion product in the system creates  $H_3O^+$  and  $OH^-$  in high concentration, thus would increase the acidity of the bulk solution<sup>13</sup>, and eases the insertion of water into the  $\beta$ -glycosidic bond that leads to hydrolysis and glucose formation. In addition, rGO as a MW sensitizer would compensate for the drop in the dielectric constant of water.

Herein, we sought to understand the structure-property-activity correlation of rGO in synergy with MW-subH<sub>2</sub>O. Individually, rGO, MW and subH<sub>2</sub>O have limitations but their integration in a single system brings about a route that has never been previously considered before. Control experiments using conventional heating and other carbon-based catalysts such as graphite and MWCNT were performed to understand the process. Furthermore, the individual contribution of rGO, MW and subH<sub>2</sub>O to the integrated system was elucidated. The proposed mechanism that best explains the process was also deduced.

## 2. Materials and methods

### 2.1 Materials

Graphite powder, sulfuric acid (98%), sodium nitrate, potassium permanganate and hydrogen peroxide (30%) for GO synthesis and glucose and 5-hydroxymethylfurfural standard reagents were all supplied by Wako Pure Chemicals Industries (Osaka, Japan). Avicel microcrystalline cellulose (MCC) as the model compound was procured from Merck USA. All chemicals were utilized as received.

### 2.2 GO/rGO synthesis

GO was synthesized following modified Hummer's method that was described in full detail in previous publication<sup>6</sup>. The reduced GO (rGO) used in this study was prepared as follows: (1) MW-hydrothermal reduction denoted as rGO1: briefly, the synthesized GO powder was subjected to MW irradiation-induced reduction using CEM Microwave Assisted Reactor system (MARS 6, CEM Matthews NC Company, USA) and XP1500 reactor (inner volume = 100ml). In this process, 1 part GO to 5 parts water were placed in the XP1500 reactor, mounted on to the holder and subjected to 200 W, at 473 K for 60min. After cooling down, the powder was filtered and dried 293 K for 48 h. (2) Thermally annealed GO denoted as rGO2 was prepared following the method stated by Voiry et al.<sup>14</sup> GO powder was heated in a tubular electric furnace under argon gas for 1 hr at 573 K.

### 2.3 Catalyst characterization

Freely settled bulk density measurement was performed using a container with a known capacity. The container was filled with the powders and was levelled off. The container was

weighed and the bulk density was calculated according to Eq. 1, where bulk density (dry, kg m<sup>-3</sup>); M: mass of the material in the container (fresh, kg); and V: volume of the empty container (m<sup>3</sup>).

$$\text{Bulk density} = MV \quad (1)$$

JEOL JSM-7600F field emission scanning electron microscopy (FESEM) was used to analyze surface morphology of the samples. Images were taken at x100 and x5000 magnifications at 2 kV filament voltage. rGO1 samples were sputter coated with gold using Quorum Technologies SC7620 Mini Sputter Coater prior to the analysis. XRD patterns were determined using Rigaku miniflex 600 and were generated with CuK $\alpha$  radiation ( $\lambda = 0.154$  nm,  $U = 40$  kV,  $I = 40$  mA) in the  $2\theta$  range of 2-600, a scan speed and scan step of 0.020. The obtained XRD patterns were analyzed using PDXL-2 was estimated following the Scherrer equation<sup>15</sup> in Eq. 2, where D: the crystallite size in nm;  $\theta$ : the Bragg angle;  $\lambda$  is the wavelength of the radiation; K: constant; and  $\beta_{1/2}$ : corrected width of the peak given by the specimen. Interlayer distance or d-spacing between GO/rGO layers was calculated using Bragg's equation<sup>16</sup> (Eq. 3). where, d: interlayer distance;  $\theta$ : angle of the diffracted wave; n: an integer known as the order of the diffracted beam; and  $\lambda$ : wavelength of incident X-ray (= 1.54 Å).

$$D_{(nm)} = \frac{K\lambda}{\beta_{1/2} \cos\theta} \quad (2)$$

$$2d \cdot \sin\theta = n\lambda \quad (3)$$

The presence of functional groups were determined by FTIR technique using JASCO FTIR 4100. The samples were milled with KBr and compacted into KBr disks. Transmittance were scanned at the wavenumber range of 4000-400cm<sup>-1</sup>. The microstructure evolution of the samples was evaluated using JASCO NRS-3100 Laser Raman Spectrophotometer. X-ray photoelectron spectroscopy (XPS) using Perkin Elmer Phi 1600 ESCA system was employed to analyze compositions. The surface area, mean pore diameter and total pore volume of the solid catalysts were measured using Belsorp mini II (BEL Japan Inc.). Samples were filled in a tube under N<sub>2</sub> atmosphere and then degassed for 24 h at 333 K prior to the measurements at 77 K using nitrogen as the adsorptive gas.

### 2.4 Catalytic depolymerization method

MW experiments were carried out using MARS 6 apparatus and XP1500. In a typical run, MCC, catalyst and distilled water at prescribed amounts were placed inside the reactor, sealed, and subjected to desired operating conditions. Temperature was measured using thermocouple. Samples were cooled down after each reaction. Liquid components (hydrolysates) and solid residues were recovered and separated via filtration in cold water bath. The residues were washed with 20 ml distilled water and dried at 333 K for 48 h prior to characterization or reuse. On the other hand, conventional heating was performed using a batch type SUS reactor (inner volume = 6 ml) and an electric heating furnace. The SUS reactor was heated to 240°C and zero time was taken when the temperature of reactor reached the set temperature, as measured by a thermocouple.

## 2.5 Product Analysis via HPLC

Products in the filtrate were identified and quantified using high performance liquid chromatography (HPLC) with a Shodex Sugar SH1011 column at a column temperature of 333 K, 0.3mM HClO<sub>4</sub> eluent at 0.5 mL/min equipped with a UV and refractive index detectors. Ten microliters of the filtrate was filtered through a syringe filter (pore size = 0.45microns) and injected into the system. Products were categorized into three: oligosaccharides, glucose and degradation products. Quantification was done using a standard calibration curve from 0.001 M to 0.5 M (R<sub>2</sub> = 0.999). Glucose yield (%GY) is defined by Eq. 4. Oligosaccharides, mostly cellobiose, was also quantified using a standard calibration curve and Eq. 4. The major glucose degradation product detected I the system is 5-hydroxymethylfurfural (5-HMF). The yield was individually calculated from the initial substrate concentration according to Eq. 5,

$$\%GY = \frac{\text{Glucose in the solution after reaction (g/L)} \times 0.9}{\text{Cellulose input (g/L)}} \times 100 \quad (4)$$

$$5HMF(\text{wt}\%) = \frac{\text{Concentration in hydrolysate } (\frac{g}{L}) \times 1.28}{\text{Initial cellulose input } (\frac{g}{L})} \times 100 \quad (5)$$

The current HPLC system/ detector used in this study was only limited to measuring oligosaccharides from cellobiose (n=2) until cellohexaose (n=6), glucose and degradation products (levulinic acid, acetic acid and 5-HMF). Hence, the carbon-balance cannot be closed.

## 3. RESULTS AND DISCUSSION

### 3.1 Characterization of rGO as a function of thermal and microwave-induced hydrothermal reduction process. The

reduction of GO through chemical or thermal methods has been widely reported since it is currently the most viable route for the synthesis of graphene for batteries, solar cells and supercapacitors application<sup>17</sup>. By visual inspection alone, notable differences can be observed amongst the catalysts in powder form. GO has a shiny brown-black color whereas rGO1 has a dull-black to grayish black color while rGO2 is deep black. The black color has been attributed to the partial restoration of the conjugation network within the carbon structure<sup>18</sup>. The bulk density of the powders also differed significantly, as shown in Table 1. Bulk density is a measure of the compaction of the powders and has an impact on the movement of water molecules and solute particles in the system<sup>19</sup>. The bulk density was found to decrease in the following order: GO>rGO1>rGO2. Since rGO2 has the lowest bulk density, it would potentially enable water molecules to diffuse better in between particles. The substantial differences between the physical properties of the synthesized rGOs prompted us to investigate whether the aqueous environment could have played a role during the reduction process. A variety of techniques were then used to further probe into the characteristics of the synthesized rGOs, as follows.

First, SEM images of GO, rGO1 and rGO2 were obtained and shown in Fig. 1. During the preparation of the specimen samples for analysis, as GO has poor conductivity, the sample was sputter-coated with gold. On the contrary, rGO1 and rGO2 did not require gold coating, demonstrating that the conductivity of rGO has been restored because of the removal of some oxygenated functionalities<sup>20</sup>. The microstructures of the samples have no significant differences at 5000x magnification (Fig. 1a-c) as they exhibit coarse and wrinkled structures containing multiple overlapping or stacked nanosheets. This observation suggests that the morphology of the carbon backbone of GO was maintained after reduction. However, at

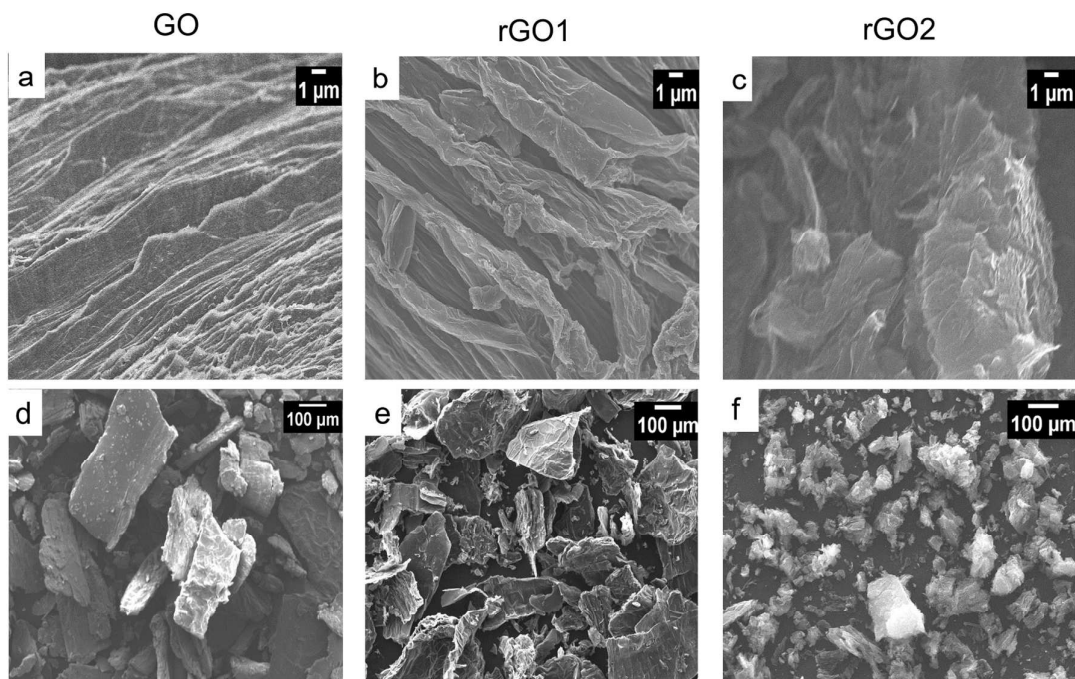


**Figure 1.** Field emission scanning electron micrographs for [a,d] graphene oxide (GO); [b,e] microwave-hydrothermal reduced GO (rGO1) and [c,f] thermally annealed GO (rGO2) @x5000 and @x100 magnification, respectively

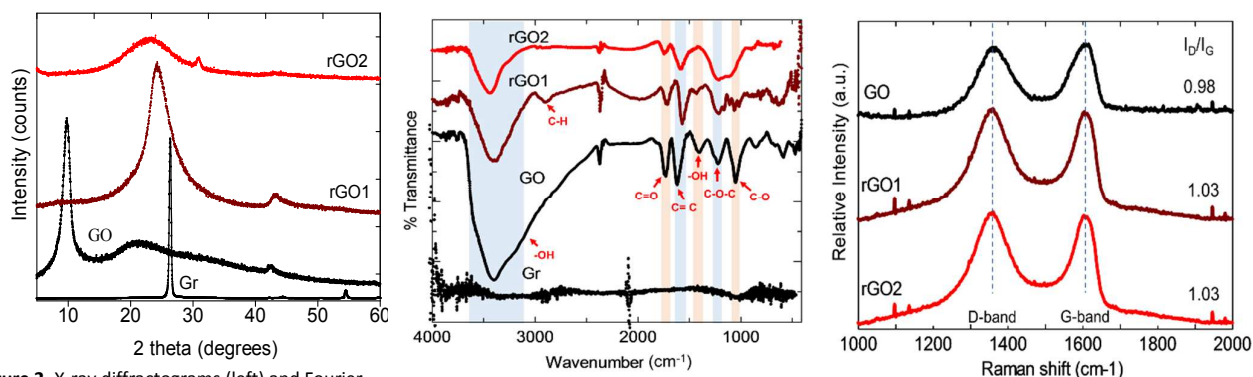


**Figure 2.** X-ray diffractograms (left) and Fourier transform infrared spectra (middle) and Raman spectra (right) obtained for graphene oxide (GO), microwave-hydrothermal reduced graphene oxide (rGO1), thermally annealed graphene oxide (rGO2) and graphite (Gr).

**Table 1.** Comparison of properties of graphene oxide (GO), microwave reduced GO (rGO1) and thermally annealed GO (rGO2)

	Bulk density, ( $\times 10^{-2}$ ), g/ml	BET surface area, $m^2/g$	Pore diameter, nm	Pore volume ( $\times 10^{-2}$ ), $cm^3/g$
GO	52.73	35	4.6	4
rGO1	22.31	31	3.2	2.5
rGO2	1.124	226	28.3	160

100x magnification, it was revealed that the particle sizes for rGO2 was much smaller than that of GO and rGO1 (Fig. 1d-f), which can be attributed to the cleaving of the GO sheets during thermal annealing<sup>21-22</sup>. For this reason, rGO2 exhibited significantly higher surface area than rGO1, as supported by BET measurements (Table 1). The larger pore diameter and greater pore volume in rGO2 can be attributed to the formation of nanopores and nanovoids arising from the cleavage of epoxy and C-C bonds<sup>23-24</sup>. Surprisingly, despite being reduced, rGO1 had slightly lower surface area, pore diameter and pore volume. This finding suggests that water molecules may have inhibited the formation of nanovoids and nanopores. Zhou et al. 2009 extensively studied the effect of hydrothermal reduction to the electronic and optical properties of rGO and concluded that the changes in dielectric properties and ion product of water under a close system of high temperature and pressure allows an effective strategy to repair the sp<sup>2</sup> network<sup>18</sup>. Next, the XRD spectra were obtained and presented in Fig. 2 (left). The starting material Gr has a very narrow peak at 26° (d-spacing = 0.34 nm) while GO has shifted its sharp peak at 10.70° (d-spacing = 0.82 nm, crystallite size = 6.7 nm). Meanwhile, rGO1 has a broad peak (d-spacing = 0.36 nm, crystallite size = 1 nm). The drop in interlayer distance value for rGO1 and rGO2 indicates that some oxygenated functionalities initially present in GO were removed, that could result into the aggregation of few layers. The reduction of crystallite size concurs with the SEM findings.

Fig.2 (middle) shows the FTIR spectra which indicates characteristic vibrational modes of functional groups. No functionalities were detected in Gr. Consistent with previous studies<sup>25-26</sup>, GO contains four sets of functionalities, that are represented as follows: hydroxyls from adsorbed water (broad O-H bond stretching vibration at  $\sim 3393\text{ cm}^{-1}$  and  $1406\text{ cm}^{-1}$ ), carbonyls and carboxyls (C=O stretching at  $1736\text{ cm}^{-1}$ , C-O stretching at  $1328\text{ cm}^{-1}$  and C=OH at  $1046\text{ cm}^{-1}$ ) and epoxides (C-O-C stretching at  $1221\text{ cm}^{-1}$ ). The C=C sp<sup>2</sup> hybridized carbons (aromatics) is assigned to  $1626\text{ cm}^{-1}$ . rGO2 showed lower intensity than rGO1 signifying better restoration of sp<sup>2</sup> with hydrothermal synthesis. For both rGO1 and rGO2, weakened intensities of the absorption bands O-H vibration at  $\sim 3393\text{ cm}^{-1}$  were observed, indicating the dehydration of rGO. The carbonyl C=O stretching at  $1736\text{ cm}^{-1}$  has also diminished. Meanwhile, rGO1 showed a peak assigned to C-H distinct to rGO2 which could be again linked to the presence of water during synthesis.

The reduction on the surface of rGO1 and rGO2 was further confirmed and evaluated using XPS measurements. XPS survey spectra are shown in Fig.S1 while the C1s and O1s positions and intensities are summarized in Table 2. The C/O ratio based from XPS analysis increased from 0.8 (GO) to 2.39 (rGO1) and 1.93 (rGO2). The combustion elemental analysis results (Table S1): C/O ratio for GO, rGO1 and rGO2 were 0.86, 3.16 and 2.64, respectively, thus both rGO contains much lower oxygen species than GO. The intensities and percentages of the various components (C=C-H, sp<sup>2</sup> and sp<sup>3</sup> carbons, C-H, C-O-C, O-C-O, quinone,  $\pi$ - $\pi^*$ , etc.) highly differ between rGO1 and rGO2. For instance, the increase in sp<sup>2</sup> carbon intensities and appearance of  $\pi$ - $\pi^*$  transitions is an indicator of the recovery of conjugated structures that were initially disturbed by an oxygenated functionality and signifies restoration of conductive properties. rGO1 has higher sp<sup>2</sup> carbon than GO as expected due to the hydrothermal reduction and more importantly, developed C-H, Csp<sup>3</sup> and C-OH than rGO2. This further supported that the presence of water has the capability to repair the defects while recovering the aromatic structures.

Furthermore, the water molecules interacted and incorporated into GO that led to the transformation of its surface structure accompanied with C-C bond cleavage in accordance to the dynamic structural model proposed by Dimiev et al.<sup>27</sup>. In order to assess structural changes particularly disorder and defects and defect density, Raman

spectra were collected. The prominent D-band ( $\sim 1360\text{ cm}^{-1}$ ) and G-band ( $1600\text{ cm}^{-1}$ ) peaks have been observed in the three samples

**Table 2.** C1s and O1s positions and intensities obtained by deconvolution for graphene oxide (GO); microwave-hydrothermal reduced GO (rGO1) and thermally annealed GO (rGO2)

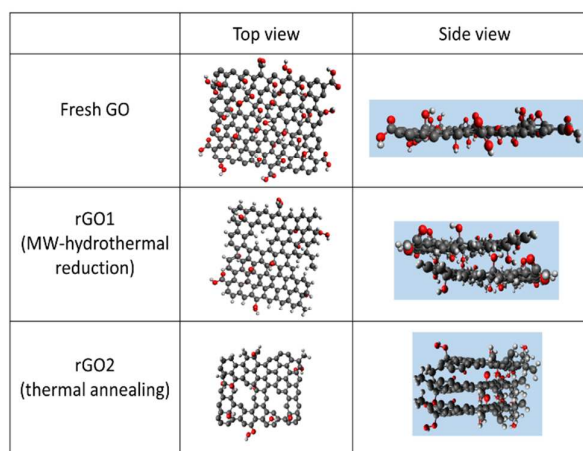
Sample	Elemental Composition (%)		C/O ratio	C1s Deconvolution									O1s Deconvolution			
	C	O		C=C-H	C=C sp <sup>2</sup>	C-H	C-C sp <sup>3</sup>	C-OH	C-O-C	C=O	O=C-O	$\pi \cdot \pi^*$	Quinone	C=O	O-C-O	C-OH
GO	44.2	55.8	0.8	8.0	41.2	-	-	41.1	-	9.7	-	-	2.7	-	-	97.3
rGO1	70.5	29.5	2.39	-	57.1	8.8	9.7	11.4	-	-	9.5	3.4	7.7	12.5	39.6	40.2
rGO2	65.9	34.1	1.93	-	66.6	-	-	17.1	7.5	-	5.7	3.1	8.8	3.1	64.4	23.7

shown in Fig. 2, right), in accordance with published studies<sup>28-29</sup>. Both rGO1 and rGO2 exhibited slight bandwidth narrowing relative to GO signifying graphitization and ordering. The ratio of intensities between D-band and G-band has been commonly used as an indicator of the extent of reduction. For GO, the ID/IG ratio is 0.98, and the smaller intensity of D-band is characteristic of oxidized state. Both rGO1 and rGO2 had similar results with ID/IG value of 1.03. This value, being higher than that of GO is indicative of the removal of the functionalities. However, the ID/IG value for rGO1 and rGO2 is lower than reported reductants such as hydrazine (2.7), vitamin C (2.3) and hydroiodic acid (2.6)<sup>30</sup>. Thus, both rGO1 and rGO2 were only partially reduced. Lastly, some functionalities still attach to both the basal plane and along the edges of rGO. It was reported that even at higher temperatures, full reduction and complete removal of these functionalities are currently impossible<sup>31</sup>.

The data obtained from the extensive characterization carried out indicated that both rGO1 and rGO2 indeed underwent partial reduction. Both suffered from the removal of oxygenated functionalities despite the difference in the preparation route. However, rGO2 possessed better surface properties suitable for catalytic applications than rGO1, owing to the nanopores and nanovoids that developed from thermal annealing. Su et al.<sup>32</sup> suggested that the nanopores and nanovoids are active sites, along with the  $\pi$ -electron system, that synergistically trap reactant molecules and facilitate reactions. The nanopores could also offer some pathway for the quick diffusion of reactant molecules and ions into the interlayer spaces<sup>33</sup>. We have constructed representative structural models of the synthesized rGO, as shown Scheme 1, using Avogadro molecule editor<sup>34</sup>. We have randomly introduced the oxygenated functionalities into GO and randomly removed them following the XPS results. The voids that formed in rGO1 was found to be rich in C-H groups including the peripheries of the sheet. The larger nanopores formed in rGO2 led to the formation of zigzag and armchair orientation which are believed to be catalytically active sites as reported in the reduction of nitroaromatic compounds<sup>35</sup>.

### 3.2 Hydrolytic Depolymerization.

The catalytic activity of rGO1 and rGO2 was tested from 473 K



**Scheme 1.** Visual representation of graphene oxide (GO); microwave-hydrothermal reduced GO (rGO1) and thermally annealed GO (rGO2) developed through Avogadro molecule editor

– 513 K. Individual contributions of MW, subcritical water and rGO1 and rGO2 were benchmarked against conventional heating and other carbon catalyst such as graphite and carbon nanotubes.

MW heating in this study takes place in two distinct circumstances, the first one is via dipolar reorientation and the second one, through interfacial polarization (also known as Maxwell-Wagner-Sillars polarization)<sup>36</sup>. Water, having permanent dipoles, interact with MW through dipolar reorientation. The dipoles reorient and rotate themselves to align with the electric field and their movement results to friction that generates heat. The interaction of water with MW, however, is affected by the changes in its properties with respect to temperature. Marshall and Franck (1981)<sup>37</sup> and Uematsu and Franck (1980)<sup>38</sup> have extensively characterized the properties of water and steam such as ion product and static dielectric constant over a wide range of temperature and pressure. Also, Cantero et. al.<sup>13</sup> plotted density, ion product and dielectric constant versus temperature to illustrate

general trends and relations. From the aforementioned references, relevant data for this study have been extracted and summarized in Table 3. Density ( $\rho$ ) signifies the quantity of water molecules per unit volume. With low density, water molecules has better diffusibility. Water molecules also have an intrinsic nature to autodissociate, forming one hydroxyl (H<sup>+</sup>) and one hydroxide (OH<sup>-</sup>) ion. The hydroxyl immediately protonates another water molecule, resulting to a hydronium ion (H<sub>3</sub>O<sup>+</sup>). The ion product (pK<sub>w</sub>) represents the extent of dissociation of water and is a measure of the H<sub>3</sub>O<sup>+</sup>/ OH<sup>-</sup> concentration inside the system. The dielectric constant ( $\epsilon$ ) describes the polarizability of molecules in an electric field<sup>39</sup>.  $\rho$ , pK<sub>w</sub> and  $\epsilon$  were found to vary inversely with temperature. More importantly, since the  $\epsilon$  value decreases as the temperature increase (Table 3), the ability of water to absorb MW also decreases.

In the absence of direct measurement of  $\epsilon$  for each of the conditions in this study, MW absorption in the system was investigated using heating rates as summarized in Table 4. Heating rates signify the increase in temperature in the system within a certain period of time. A high heating rate value is crucial such that the desired temperature was attained at a shorter period of time and is favorable to minimize unnecessary reactions and byproduct formation<sup>40</sup>. It should be noted that in all conditions tested under MW heating, the heating rates were found to slow down as temperature is increased. This observation highly correlates with the observed decrease of  $\epsilon$ . Thus, under uncatalyzed conditions, corresponding heating rates are generally low (0.86 – 0.59 K/s). The introduction of rGO1 increased the heating rates (1.28 – 0.88 K/s). This indicates that the presence of carbon-based catalyst helped overcome the change in the dielectric constant of water, thus, enabling heating to proceed steadily. Carbon-based catalysts interact with MW through interfacial polarization, wherein the movement of electrons essentially matters. Therefore, rGO2 induced much better heating rates than rGO1 as expected, and is attributed to its marginal oxygenated functionalities content. Moreover, the electron transfer ability is enhanced due to its higher sp<sup>2</sup> carbon than rGO1 as discussed earlier. Indeed, both rGO1 and rGO2 has better heating rates than GO which we previously reported as 1.06 K/s.

**Table 3.** Properties of subcritical water for the conditions stated in this study.

Temperature (K)	Saturated Vapor Pressure P <sub>sat</sub> , kPa	Density, $\rho$ , kg/m <sup>3</sup>	Log <sub>10</sub> (ion product), pK <sub>w</sub>	Dielectric constant, $\epsilon$
298	3.169	997	13.995	78.85
473	1553.8	864.3	11.210	35.11
493	2318	840.3	11.153	31.93
513	3344	813.7	11.103	28.91

**Table 4.** Calculated heating rates for all combinations used in this study

Temp. (K)	Heating Rates (K/s)					
	MW-subH <sub>2</sub> O	rGO1 + MW-subH <sub>2</sub> O	rGO2 + MW-subH <sub>2</sub> O	CNT + MW-subH <sub>2</sub> O	Gr + MW-subH <sub>2</sub> O	ch-subH <sub>2</sub> O
473	0.86	1.28	1.50	1.10	0.70	0.68
493	0.62	1.09	1.30	0.96	0.58	0.59
513	0.59	0.88	1.08	0.82	0.44	0.47

[MW – microwave; subH<sub>2</sub>O – subcritical conditions; rGO1 – microwave-hydrothermal reduced GO; rGO2 – thermally annealed GO (rGO2); CNT – carbon nanotubes; GR – graphite; ch – conventional heating]

(Reaction conditions: 1:1:50 cellulose: catalyst: distilled water, ramped from room temperature to desired temperature and zero holding time, 200 W, with stirring)

The heating rates has implications on the heating up time. With MW-subH<sub>2</sub>O, the desired temperatures were achieved between 8-15 min. Just the heating time alone is already twice or thrice longer than the actual reaction time of 5 min. In the presence of rGO1, heating up was about 15-35% faster than MW-subH<sub>2</sub>O heating. While CNT has also improved MW absorbance of the system, both rGO1 and rGO2 were better. Gr, on the other hand, had the lowest heating rates amongst the carbon catalysts tested as it reflects considerable amount of MW<sup>41</sup>. Thus, not all carbon-based catalysts could be exceptional MW sensitizers. In the absence of direct measurement of dielectric constants for carbon catalysts, heating rates could serve as a measure of MW-catalyst interaction. Moreover, as temperature is increased, heating rates slows down regardless of the presence of catalyst. It should also be noted that the ability of carbon catalysts to absorb microwave also decreases as temperature is increased<sup>42</sup>.

Heating rates under conventional method is quite different from MW-induced ones. Under ordinary heating circumstances, calculated heating rates was <0.1 K/s. The rather slow heating rate was due to conduction and heat transfer resistance. In order to speed up heating, two heating furnaces were used; the first one was set to a temperature much higher than the desired temperature, i.e. 623 K, where the heating up was carried out. The second furnace was maintained at the target temperature, i.e. 473 K – 513 K, where the reaction was carried out. Heating rates were obtained from the first furnace and once the equilibrium temperature was reached, the reactor was immediately transferred to the second furnace and maintained there for 5 min. The reactor was immediately quenched to suppress any side reactions. The large temperature gradient had enabled heating rates to be comparable with MW-subH<sub>2</sub>O but was a huge wastage of energy. Even so, the time spent for just heating up was about three to four times longer than the actual reaction time of 5min. Similarly, the heating rate for conventional system slowed down as the temperature gradient between the system and the furnace became smaller.

### 3.3 Product distribution and yields.

Useful insights were also obtained from the representative HPLC chromatograms as shown in Fig. S2. A two-step model of cellulose depolymerization would typically indicate the

formation of soluble oligosaccharides and soluble sugars<sup>43</sup>. The products formed during the depolymerization reaction as determined by HPLC peaks was categorized into: (i) oligosaccharides, displayed prior to ~16min; (ii) glucose, assigned to peaks at ~16min; and (iii) 5-HMF, as labeled to peaks at ~39min.

Comparing ch-subH<sub>2</sub>O and MW-subH<sub>2</sub>O, soluble products were not detected for both at 473 K. Only MW-subH<sub>2</sub>O showed glucose peaks at 493 K while both managed to produce glucose at 513 K. Since both system is under the same temperature, it can be established that the heating source indeed affects the depolymerization process. Fan et al. attributed the observed superiority of MW-induced depolymerization process with the CH<sub>2</sub>OH pendant groups acting as molecular radiators that initiated cleavage of the biopolymer chain<sup>44</sup>. The CH<sub>2</sub>OH pendant groups also facilitated conformational arrangement that promoted accessibility of the β-1,4 glycosidic bond.

In solid-solid reactions, the diffusion of the reactants is the slowest step and thus, governs rate of reaction. At 473 K, Gr and CNT did not manage to produce glucose. For CNT, this result was unexpected since CNT and rGO shares the same sp<sup>2</sup> hybridization. It was earlier reported that flat structural properties as that of rGO offer advantages since it has lower diffusion resistance compared with CNT that may have restriction at tube ends<sup>40</sup>. On the other hand, rGO1 managed to generate glucose with minimal oligosaccharides while rGO2 generated more glucose and higher oligosaccharides. This finding indicates that rGO2 has accelerated the depolymerization process better than rGO1. The cleavage of GO sheets during the thermal treatment generated smaller rGO sheets resulting to large amount of edges<sup>21</sup> and nanopores, that has enabled the easy diffusion of the oligosaccharides and the highly reactive hydronium and hydroxyls into the nanopores of rGO2 and in between rGO2 particles. Thus, rGO2 has led to a more precise cleaving of the C-O glycosidic bond. The enhanced binding of natural biomolecules including cellulose dimer is with rGO than with GO has been illustrated by Radic et al.<sup>45</sup> using a dynamic modelling.

At 493 K, all carbon catalysts generated glucose with oligosaccharides, whereas rGO1 and rGO2 has demonstrated better selectivity to glucose with oligosaccharides that were below quantification limits. Finally at 513 K, all catalysts managed to generate glucose with small quantities of 5-HMF. At this temperature, the contribution of subH<sub>2</sub>O was highlighted since there is an abundance of hydroxyls and hydronium ions in the system. Aside from the glucose formation, selectivity is enhanced. However, the reactive nature of glucose especially at 513 K, led to its conversion into 5-HMF.

The complete product distribution yields are summarized in Table S2. The calculated glucose yields were then illustrated in Fig. 3. Overall, the yield of glucose under the investigated temperatures range increases as temperature is increased, owing to the combined weakening of cellulosic hydrogen bonding network and the auto-dissociation of water. ch-subH<sub>2</sub>O yielded the lowest glucose yield which was improved by the presence of rGO1 and rGO2. Under conventional heating, rGO2 seemed to perform poorer than rGO1, and this could be associated to the bulkiness of rGO2 that filled up and occupied the entire length of the SUS

reactor. This may have restricted the interaction of the bulk cellulose particles with the other rGO2 catalysts and water along the length of the SUS reactor. MW-subH<sub>2</sub>O generated 11.5± 0.1% produced at 513 K which was close to the 14% reported by Fan et al., at 533 K. This yield was surpassed with rGO1 and rGO2 at 493 K, 15±4.2% and 38±7%, respectively, indicating that the presence of the catalyst has enabled depolymerization at lower temperature. In addition, the yield of rGO1 with conventional heating and with MW assistance appears to be almost the same. However, it should be noted that under conventional heating, the heating up time is about 18 min, which is only about 8 min under MW irradiation. Hence, MW assisted conditions has made significant contribution in shortening the heating up time and eventually the total process time. At 513 K, yields rose to 36±4% and 65.5±3.7% for rGO1 and rGO2, respectively. CNT+ MW-subH<sub>2</sub>O and Gr+ MW-subH<sub>2</sub>O performed poorly compared with

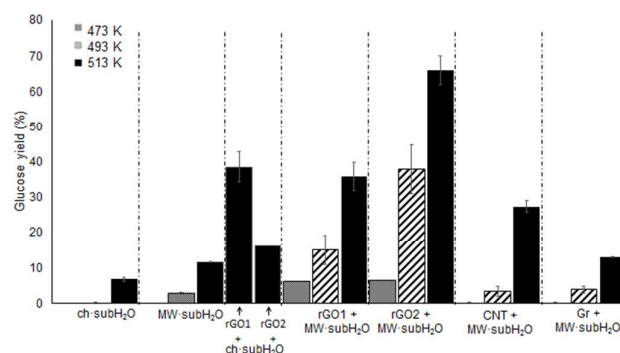


**Figure 3.** Summary of glucose yields under all conditions tested in this study [MW – microwave; subH<sub>2</sub>O – subcritical conditions rGO1 – microwave-hydrothermal reduced GO; rGO2 - thermally annealed GO (rGO2); CNT – carbon nanotubes; GR – graphite; ch – conventional heating]

(1:1 cellulose: catalyst by weight; 10ml water; 200 W microwave power, holding time of 5 minutes and 473 – 513 K)

rGO+MW-subH<sub>2</sub>O. The shorter reaction time eases concerns with the use of higher temperatures. The 5 min reaction time was used following an Arrhenius-type temperature dependency profile.

In Table S3 of the supplementary material, a summary of the performance of rGO2 in comparison with other carbon-based catalysts was provided. The glucose yields obtained in the present study is second to the yields produced by Prof. Fukuoka's group involving mechanocatalytic approach and mix-milling. Their work however entails a separate pre-treatment step for the process intensification scheme. Both studies however, has focused not only on the catalyst structure alone but also techniques to further improve yields. Tolonen et al.<sup>43</sup> has also extensively studied whether subcritical water has dissolved cellulose polymer. If the cellulose has dissolved in MW-subH<sub>2</sub>O with or without rGO, the formation of a cellulose allomorph, or Cellulose II as a precipitate, would have been observed in the hydrolysate. None of the hydrolysates produced any precipitate even after several days, hinting that solubilization did not take place.

### 3.4 Spent rGO characterization and reuse

The solid residue at the end of each rGO2-run were collected and characterized. The recovered solid residue closely resembles fresh rGO2 with a slightly paler black color. However, the mass of the collected solid residue was greater than the input rGO2, indicating the presence of unconverted cellulose. Thus, for this reason, the calculation of conversion and selectivity cannot be accurately obtained. Selectivity should be obtained from reactant conversion rather than from soluble liquid products, following the guidelines stipulated by Hammond, 2017<sup>46</sup>.

The spent rGO2 was also utilized for a subsequent run (Fig. 4, CYC 2\_pure). When used as it is, the yield for the second run was found to decrease from 66% to 43%. This may be attributed to the combined effects of the further removal of the remaining oxygenated functionalities and the blocking of the nanopores and nanovoids due to small cellulose unconverted residues. This can be resolved by mixing fresh rGO2 with spent rGO2 to minimize the decrease in yields. In order to support this claim, additional experiments were then carried out. The catalyst used for a subsequent run consisted of 50% fresh rGO and 50% residue from a previous run, as depicted in Fig. S3. As shown in Fig. 4, for the second cycling (CYC2\_50%), glucose yield reached ~55% while the third cycling (CYC3\_50%) reached ~52%, indicating that the addition of fresh rGO2 could indeed help improve catalyst performance upon reuse.

The collected residues after each cycling were subjected to XRD, FTIR and XPS analyses to provide some explanation for the decrease in yield (Refer to Fig. S4 and S5 and Table S4). The FTIR showed weaker signals for almost all functionalities present originally present in rGO2, confirming further removal of oxygenated groups. The XRD, on the other hand, illustrated broad peaks representative of rGO. The amount of oxygen groups were quantified using XPS and the C:O ratio was found to increase, from 1.9 to the first cycle to 3.3 the third cycle, reaffirming loss of oxygenated functionalities. It has been reported that carbonized cellulose produce sheet-like structure containing aromatic domain, similar to graphene, with aromatic domains between 1.2 – 1.3 nm<sup>47</sup>. Such nanovoids were much smaller than that of rGO2 hence, it cannot fully contribute to the depolymerisation process. Thus, the removal of the remaining oxygenated functionalities and presence of carbonized cellulose were likely reasons for the decrease in catalytic activity of the spent rGO2.

### 3.5 Insights to mechanism

The key step for a successful cellulose depolymerization into glucose involves the C-O glycosidic bond cleavage, which can be facilitated by Bronsted acids. In so far, there are two mechanisms, namely, surface attrition and random scission that has been proposed to explain the occurrence of glucose formation from cellulose via hydrolytic cleaving. In surface attrition, the bulk crystalline structure is peeled layer by layer resulting to shorter soluble chains that easily hydrolyze<sup>22</sup>. Under this mechanism, the formation of oligosaccharides is almost negligible and the formation of degradation products is rather slow. Surface attrition is typically associated with surface reactions or depolymerization with solid catalysts. On the other hand, in random scission, dominant hydrolysis reaction leads to the formation of oligosaccharides at various chain length.  $\beta$ -glycosidic bonds are typically attacked by H<sup>+</sup> from homogeneous acid or H<sub>3</sub>O<sup>+</sup> from the autodissociation of water<sup>48</sup>.

Based from our results as discussed above, we speculated that the possible mechanism takes place via random scission. The rupture of the C-O glycosidic bond initially produced oligosaccharides, which was further hydrolyzed to give glucose.

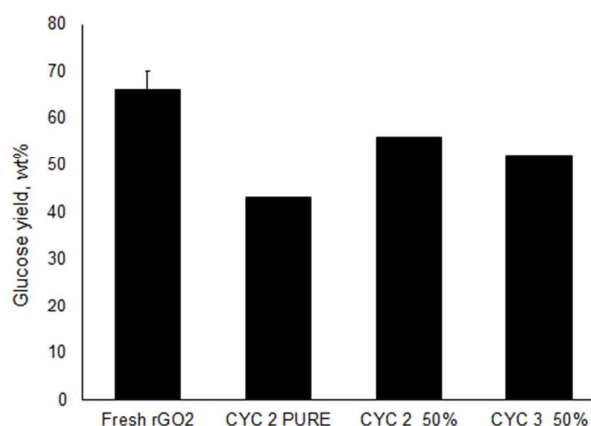
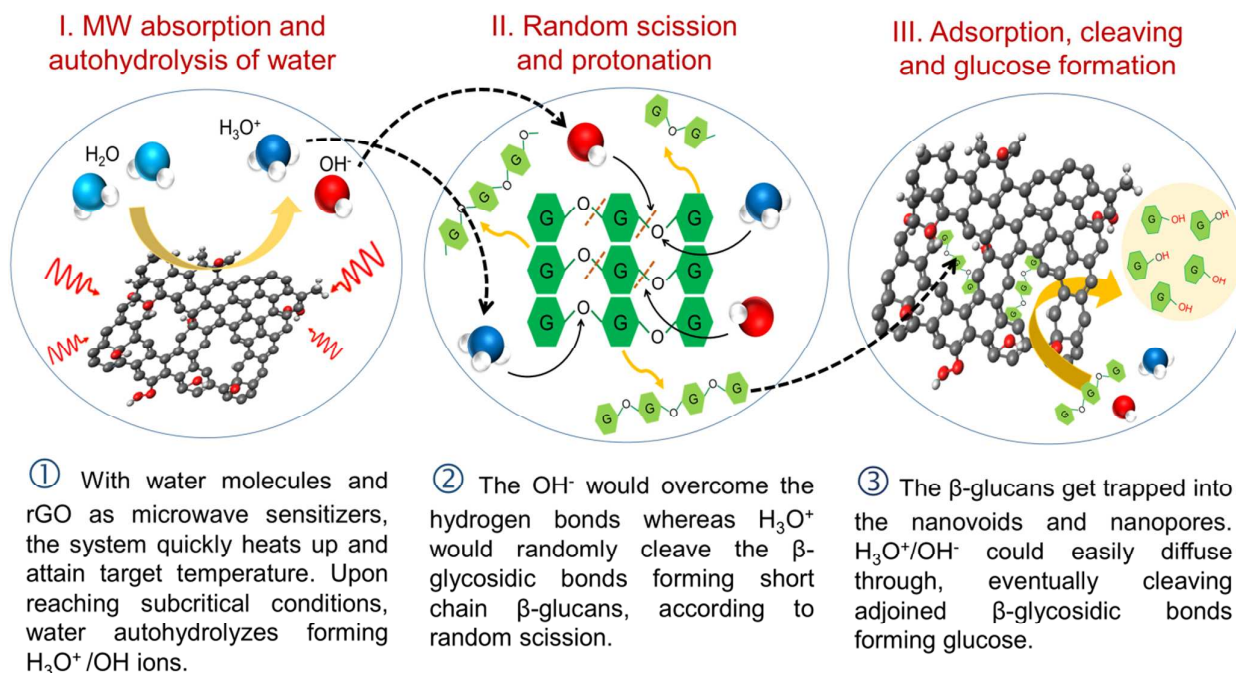


Figure 4. Catalyst reusability study as a function of glucose yield



**Scheme 2.** Proposed reaction mechanism depicting random scission under the synergy of microwave irradiation, reduced graphene oxide and subcritical water

Scheme 2 illustrates the sub-stages involved in the whole depolymerization process. First, rGO and water molecules absorb supplied MW, rapidly heating the bulk solution. As the temperature reach past 473 K, drastic decrease in the dielectric constant of water took place slowing down MW absorbance.

Consequently, water underwent auto-dissociation resulting to the formation of  $\text{H}_3\text{O}^+/\text{OH}^-$ . The largest  $\text{H}_3\text{O}^+/\text{OH}^-$  concentration was achieved at 513 K. The  $\text{H}_3\text{O}^+/\text{OH}^-$  would randomly cleave the  $\beta$ -glycosidic bonds, forming shorter chain oligosaccharides that can be trapped or adsorbed within the pores or defects of rGO. The  $\text{H}_3\text{O}^+/\text{OH}^-$  would easily diffuse through the rGO nanopores, further cleaving the oligosaccharides, eventually forming glucose monomers. Due to the highly reactive nature of glucose, formation of 5-HMF is inevitable, particularly at 513 K. In the proposed reaction mechanism, it was suggested that  $\beta$ -glucans or oligosaccharides could be trapped in between the nanopores and nanovoids of the rGO2 which could have facilitated faster hydrolysis reaction. We measured the particle size of cellobiose, which was the most detected oligosaccharides or  $\beta$ -glucans, as per HPLC analysis. We have prepared a solution of cellobiose and measured the particle size using dynamic light scattering technique (DLS). A representative histogram distribution of the particle size measurement is shown in Fig. S6 wherein cellobiose particle sizes ranged from 0.6 to 5560 nm with an average of 56 nm. With nanopore average of about 28 nm, it is possible that cellobiose having particle size at the lower segment of the distribution could be trapped into the nanovoids as suggested.

Combining the present analyses with our previous work, we have illustrated the synergism of MW, carbo-carbocatalysis and water towards cellulose depolymerization with respect to

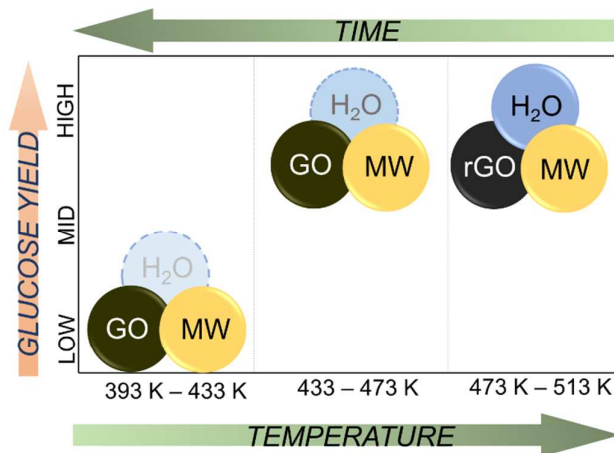


**Figure 5.** Integrated effects of microwave (MW), water ( $\text{H}_2\text{O}$ ) and graphene based catalysts on glucose yield with respect to temperature and time (GO – graphene oxide; rGO – reduced graphene oxide)

temperature, time and glucose yield in Fig. 5. Despite the presence of GO at slightly elevated temperatures (393– 433 K), yields were low and takes significantly long time to attain. This was due to insufficient ability of the temperature to soften hydrogen bonds and the inadequacy of the weak-acid surface functionalities in GO to enable hydrogen bond disruption, limiting the hydrolysis only of available amorphous regions. When temperature was increased from 433– 473 K, at reasonable length of time, the highest glucose yields could be obtained. The elevated temperatures enabled better interact

with cellulose, allowing for surface attrition to take place. At subcritical conditions, i.e. 473 – 513 K, rGO can be used to generate moderately high yields. Since depolymerization took place at very short times, yield can be increased by running several cycles over a certain period of time.

## Conclusions

In summary, we have successfully demonstrated that rGO can be used to catalyze reactions in synergy with subcritical water under microwave irradiation even without functionalization. rGO acted as microwave sensitizer to complement the changes in dielectric properties of water and as adsorption sites owing to the nanopores and nanovoids developed during its synthesis process. The product yield is also governed by the synthesis method for rGO, wherein, an atmosphere of inert gas is better than hydrothermal process. The restoration of the sp<sup>2</sup> hybridization on the rGO surface facilitated electron mobility, resulting to higher heating rates in the system. rGO has facilitated precise cleaving of the C-O glycosidic bond, much better than graphite or carbon nanotubes. Microwave has accelerated the reaction by cutting down on heating up time and also enabling conformational changes leading to the cleaving of glycosidic bond. Subcritical water has loosened the hydrogen bonding at the surface of cellulose and provided an environment rich of highly reactive H<sub>3</sub>O<sup>+</sup>/OH<sup>-</sup> that could easily diffuse into the nanopores and in between rGO particles, readily accessing sites for protonation.

## Conflicts of interest

“There are no conflicts to declare”.

## Acknowledgements

We gratefully acknowledge financial support for this research from the Japan Science and Technology Agency via the e-ASIA joint research program in the field of Functional Materials (Grant Number: 14528300). The authors also acknowledge the assistance of Dr. Michio Koinuma on the XPS analyses of GO, Mr. Jonas Karl Agutaya on the use of Avogadro molecule editor and Mr. Jomari Angel Jacinto for preparation of rGO<sub>2</sub>.

## Notes and references

- 1 Y. Huang and Y. Fu, *Green Chem*, 2013, 15, 1095-1111
- 2 D.M. Alonso, J.Q. Bond, J. Q. and J.A. Dumesic, *Green Chem*, 2010, 1493.
- 3 C.K. Chua and M. Pumera, *Catalysis. Chem. – Eur. J.* 2015, 21, 12550-12562.
- 4 J.S. Luterbacher, D. Martin Alonso, and J.A. Dumesic, *Green Chem*, 2014, 16, 4816-4838.
- 5 R. Rinaldi and F. Schüth, *Energy Environ. Sci.*, 2009, 2, 610-626.
- 6 E.G. Mission, A.T. Quitain, A. T., M. Sasaki and T. Kida, *Green Chem*. 2017, 19, 3831-3843.
- 7 J.L. Figueiredo, J. L. and M.F. Pereira. *Catalysis Today*, 2010, 150(1-2), 2-7.
- 8 L. Li, P.A. Quinlivan and D.R. Knappe, *Carbon*, 2003, 41(8), 1693. doi:10.1016/s0008-6223(03)00121-0
- 9 Y. Wu, Z. Fu, D. Yin, Q. Xu, F. Liu, C. Lu, and L. Mao, *Green Chem*, 2010, 12, 696-700.
- 10 J. Zheng, H. Liu, B. Wu, C. Di, Y. Guo, T. Wu, ... D. Zhu, *Scientific Reports* 2012, 2(1).
- 11 Y. Sugano, M.C. Vestergaard, M. Saito, M. and E. Tamiya, *Chemical Comm.* 2011, 47, 7176.
- 12 M. Yabushita, H. Kobayashi, and A. Fukuoka, *Appl. Catal. B: Environ.* 2014, 145, 1-9.
- 13 D.A. Cantero, A. Sánchez Tapia, M.D. Bermejo and M.J. Cocero, *Chem. Eng. J.* 2015, 276, 145-154.
- 14 D. Voiry, J. Yang, Kupferberg, R. Fullon, C. Lee, H.Y. Jeong, H.S. Shin and M. Chhowalla, *Science* 2016, 353, 1413-1416.
- 15 G. Zhu, X. Zhu, Q. Fan, X. Wan, J. *Anal. Appl. Pyrolysis* 2011, 90, 182-186.
- 16 Y. Sheng, X. Tang, E. Peng, J. Xue, *J. Mater. Chem. B* 2013, 1, 512-521.
- 17 F.T. Johra, W. Jung, *Appl. Surf. Sci.* 2015, 357, 1911-1914
- 18 Y. Zhou, Q. Bao, L.A. Tang, Y. Zhong, K.P. Loh, *Chemistry of Materials* 2009, 21, 2950-2956.
- 19 E. Abdullah and D. Geldart, *Powder Technology* 1999, 102, 151-165.
- 20 J. Guerrero-Contreras and F. Cabballero-Briones, *Mater. Chem. Phys.* 2015, 153, 209-220.
- 21 N. Morimoto, K. Morioku, H. Suzuki, Y. Nakai, Y. Nishina, *Chem. Commun.* 2017, 53, 7226-7229.
- 22 H. Zhao, J. Wang, D. Zhang, Q. Dai, Q. Han, P. Du, C. Liu, Y. Xie, Y. Zhang, H. Co, Z. Fan, *Sci. Rep.* 2017, 7:42643, 1-11.
- 23 L. Lin and J.C. Grossman, *Nat. Commun.* 2015, 6:8335, 1-7.
- 24 N. Kim, G. Xin, S. Cho, C. Pang, H. Chae, *Current Applied Physics* 2015, 15, 953-957.
- 25 M. Li, C. Liu, Y. Xie, H. Cao, H. Zhao, Y. Zhang, *Carbon* 2014, 66, 302-311.
- 26 G. Shao, Y. Lu, F. Wu, C. Yang, F. Zeng, Q. Wu, *J. Mater. Sci.* 2012, 47, 4400-4409.
- 27 A.M. Dimiev, L.B. Alemany and J.M. Tour, *ACS Nano* 2012, 7, 576-588.
- 28 H. Sun, S. Liu, G. Zhou, H.M. Ang, M.O. Tadé, S. Wang, *ACS Appl. Mater. Interfaces* 2012, 4, 5466-5471.
- 29 H.R. Thomas, S.P. Day, W.E. Woodruff, C. Vallés, R.J. Young, I.A. Kinloch, J.P. Rourke, *Chem. Mater.* 2013, 25, 3580-3588.
- 30 S. Eigler, S. Grimm, M. Enzelberger-Heim, P. Müller, A. Hirsch, *Chem. Commun.* 2013, 49, 7391.
- 31 V. V. Chaban and O.V. Prezhdo, *Nanoscale*, 2017, 9 (11), 4024-4033.
- 32 C. Su, M. Acik, K. Takai, J. Lu, S. Hao, Y. Zheng, P. Wu, Q. Bao, T. Enoki, Y.J. Chabal, K. Ping Loh, *Nat. Commun.* 2012, 3:1298, 1-9.
- 33 C. Chen, N. Pu, Y. Liu, L. Chen, C. Wu, T. Cheng, M.H. Lin, M. Ger, Y. Gong, Y. Peng, M. Grubb, R.T. Chen, *Composites Part B: Engineering* 2018, 135, 119-128.
- 34 Avogadro: an open-source molecular builder and visualization tool. Version 1.XX. <http://avogadro.cc/>
- 35 H. Hu, J.H. Xin, H. Hu, X. Wang, *Nano Res.* 2015, 8, 3992-4006.
- 36 T. Kim, J. Lee, K. Lee, *Carbon letters* 2014, 15, 15-24.
- 37 W.L. Marshall and E.U. Franck, *J. Phys. Chem. Ref. Data* 1981, 10, 295-304.
- 38 M. Uematsu and E.U. J. *Phys. Chem. Ref. Data* 1980, 9, 1291-1306.
- 39 S. Tsubaki, M. Hiraoka, S. Hadano, K. Okamura, T. Ueda, H. Nishimura, K. Kashimura, T. Mitani, *Carbohydr. Polym.* 2014, 115, 78-87.
- 40 T. Rogalinski, K. Liu, T. Albrecht, G.J. Brunner, *Supercrit. Fluids* 2008, 46, 335-341.

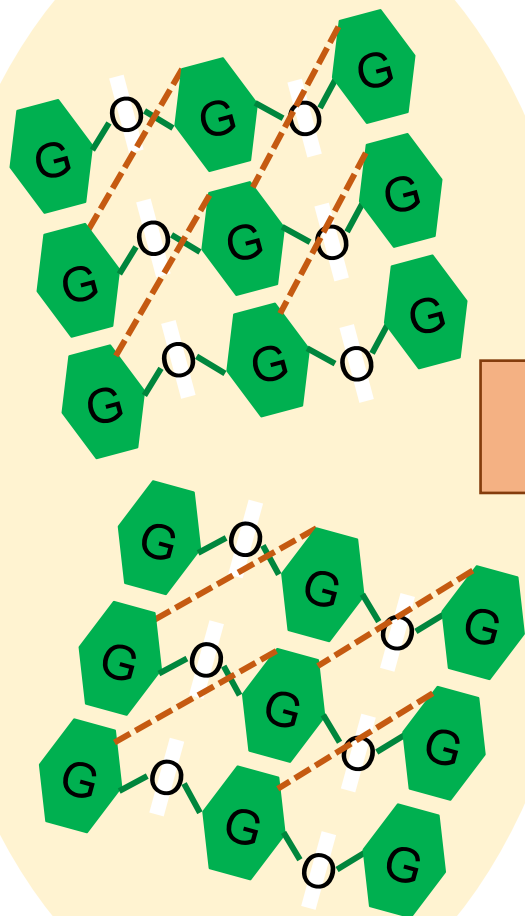
## Journal Name

## ARTICLE

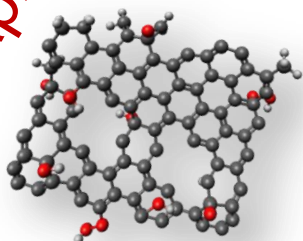
- 41 J. Menéndez, A. Arenillas, B. Fidalgo, Y. Fernández, L. Zubizarreta, E. Calvo, Bermúdez, *Fuel Processing Technology* 2010, 91, 1-8.
- 42 N. Cai and P. Larese-Casanova, *J. Environ. Chem. Eng.* 2016, 4, 2941-2951.
- 43 L.K. Tolonen, M. Juvonen, K. Niemelä, A. Mikkelsen, M. Tenkanen, H. Sixta, *Carbohydr. Res.* 2015, 401, 16-23
- 44 J. Fan, M. De bruyn, V.L. Budarin, M.J. Gronnow, P.S. Shuttleworth, S. Breeden, D.J. Macquarrie, J.H. Clark *J. Am. Chem. Soc.* 2013, 135, 11728-11731.
- 45 S. Radic, N.K. Geitner, R. Podila, A. Käkinen, P. Chen, P.C. Ke, F. Ding, *Sci. Rep.* 2013, 3:2273,
- 46 C. Hammond, *Green Chemistry*, 2007, 19(12), 2711-2728.
- 47 J. Matthiesen, T. Hoff, C. Liu, C. Poeschel, R. Rao, J. Tessonnier *Chinese Journal of Catalysis*, 2014, 35(6), 842-855.
- 48 Y. Yu and H. Wu, *Ind. Eng. Chem. Res.* 2010, 49, 3919-3925.

random scission

cellulose



reduced graphene oxide



adsorption site

microwave absorber

bond breaking

protonation

rapid heating

conformational changes

microwave irradiation

subcritical H<sub>2</sub>O

glucose

